

Characterizing gravitational instability in turbulent multicomponent galactic discs

Oscar Agertz,¹[★] Alessandro B. Romeo² and Kearn Grisdale¹

¹*Department of Physics, University of Surrey, Guildford, GU2 7XH, UK*

²*Department of Earth and Space Sciences, Chalmers University of Technology, SE-41296 Gothenburg, Sweden*

Accepted 2015 February 24. Received 2015 February 19; in original form 2014 December 20

ABSTRACT

Gravitational instabilities play an important role in galaxy evolution and in shaping the interstellar medium (ISM). The ISM is observed to be highly turbulent, meaning that observables like the gas surface density and velocity dispersion depend on the size of the region over which they are measured. In this work, we investigate, using simulations of Milky Way-like disc galaxies with a resolution of ~ 9 pc, the nature of turbulence in the ISM and how this affects the gravitational stability of galaxies. By accounting for the measured average turbulent scalings of the density and velocity fields in the stability analysis, we can more robustly characterize the average level of stability of the galaxies as a function of scale, and in a straightforward manner identify scales prone to fragmentation. Furthermore, we find that the stability of a disc with feedback-driven turbulence can be well described by a ‘Toomre-like’ Q stability criterion on all scales, whereas the classical Q can formally lose its meaning on small scales if violent disc instabilities occur in models lacking pressure support from stellar feedback.

Key words: instabilities – turbulence – ISM: general – ISM: kinematics and dynamics – ISM: structure – galaxies: ISM.

1 INTRODUCTION

Today, over three decades after the pioneering work by Larson (1981), observations and simulations of the interstellar medium (ISM) are revealing its turbulent nature with higher and higher fidelity (see review by e.g. Elmegreen & Scalo 2004; Mac Low & Klessen 2004). Turbulence is not only thought to play an important role in controlling star formation in molecular clouds (McKee & Ostriker 2007; Padoan & Nordlund 2011; Federrath & Klessen 2012), but also on galactic scales (Renaud et al. 2013) and in shaping the ISM (Stanimirovic et al. 1999; Elmegreen, Kim & Staveley-Smith 2001; Bournaud et al. 2010). The importance of galactic-scale turbulence has in the past decade also been revealed in the early Universe; in gas-rich high-redshift galaxies, the observed levels of gas turbulence are much higher than in the local Universe (Shapiro et al. 2008; Förster Schreiber et al. 2009; Swinbank et al. 2011), explaining the observed ubiquity of supermassive star-forming clumps (Agertz, Teyssier & Moore 2009b; Bournaud & Elmegreen 2009; Dekel, Sari & Ceverino 2009; Elmegreen et al. 2009; Genzel et al. 2011).

One of many fundamental aspects of ISM turbulence is the existence of scaling relations between observables, such as the column

density (Σ), the 1D velocity dispersion (σ), and the size of the region (ℓ) over which such quantities are measured:

$$\Sigma \propto \ell^a, \quad \sigma \propto \ell^b. \quad (1)$$

The values of exponents a and b depend on which ISM component and the range of scales that are considered. In this work, we focus mainly on the cold neutral gas; neutral hydrogen (H I), and molecular gas, dominated by molecular hydrogen (H_2 , observed via the tracer molecule CO), which is known to be supersonically turbulent and plays an important role in the gravitational instability of galactic discs (e.g. Lin & Shu 1966; Jog & Solomon 1984; Bertin & Romeo 1988).

In molecular gas, the scaling exponents are $a \approx 0$ and $b \approx \frac{1}{2}$, up to scales of several 100 pc.¹ This pair of exponents are often referred to as ‘Larson’s scaling laws’ after the discovery by Larson (1981, see also Solomon et al. 1987). In fact, both Galactic and extragalactic Giant Molecular Clouds (GMCs) are fairly well described by Larson’s scaling laws, although with large uncertainties (e.g. Bolatto et al. 2008; Heyer et al. 2009; Hughes et al. 2010; Kauffmann et al. 2010; Lombardi, Lada & Alves 2010; Roman-Duval et al. 2010; Sánchez et al. 2010; Ballesteros-Paredes et al.

¹ Note that $a = 0$ is expected for isolated clouds in gravitational equilibrium, as the cloud mass $M \propto \ell \sigma^2$ together with $\sigma \propto \ell^{0.5}$ gives $\Sigma \sim M/\ell^2 = \text{constant}$.

* E-mail: o.ageritz@surrey.ac.uk

2011; Beaumont et al. 2012), as well as in the dense star-forming clumps in high-redshift galaxies (Swinbank et al. 2011).

Simulations of GMCs forming in galactic discs have recently started producing scaling relations compatible with Larson's relations (e.g. Hopkins, Quataert & Murray 2012; Dobbs 2015), but see Fujimoto et al. (2014) for models predicting steeper relations ($\Sigma(\ell)$, $\sigma(\ell) \propto \ell$). State-of-the-art numerical simulations of supersonic turbulence suggest $a \sim \frac{1}{2}$ and $b \sim \frac{1}{2}$ (Fleck 1996; Kowal & Lazarian 2007; Kritsuk et al. 2007; Schmidt, Federrath & Klessen 2008; Price & Federrath 2010; Kritsuk, Lee & Norman 2013). Other recent numerical work suggest that the scaling exponent a may be significantly affected by the nature of the turbulence forcing (Federrath et al. 2010), magnetic fields, and self-gravity (Collins et al. 2012).

In H I, the scaling exponents are $a \sim \frac{1}{3}$ and $b \sim \frac{1}{3}$ up to several kpc (Roy, Peedikakkandy & Chengalur 2008), although, as for molecular gas, with large uncertainties (Kim et al. 2007). Observed power spectra of H I intensity fluctuations in nearby galaxies are compatible with a Kolmogorov scaling for both σ and Σ (e.g. Stanimirovic et al. 1999; Lazarian & Pogosyan 2000; Elmegreen et al. 2001; Begum, Chengalur & Bhardwaj 2006; Bournaud et al. 2010; Zhang, Hunter & Elmegreen 2012; Dutta et al. 2013), with similar results for other ISM components on large scales (e.g. dust and CO in M33; Combes et al. 2012). Furthermore, H I power spectra are often found to be shallower on large scales, with a break around $\ell \sim$ the disc scaleheight, possibly indicating a transition from 3D turbulence on small scales to 2D turbulence on large (Dutta et al. 2008, 2009; Block et al. 2010; Bournaud et al. 2010).

While the turbulent nature of the ISM is well established, it is rarely accounted for in theoretical works when evaluating the gravitational stability of galactic discs. Instead, σ and Σ are associated with smoothed quantities on galactic scales (\sim kiloparsecs; but see Elmegreen 1996; Begelman & Shlosman 2009; Hopkins 2012). A few analytical studies investigating the effect of ISM turbulence on gravitational stability have been carried out. Romeo et al. (2010) explored a range of values for a and b and showed that turbulence has an important effect on the gravitational instability of the disc; it excites a rich variety of stability regimes, several of which have no classical counterpart. Follow-up studies by Hoffmann & Romeo (2012) and (Romeo & Falstad 2013, see also Shadmehri & Khajenabi 2012) extended this framework to turbulent multicomponent (gas+stars) discs and applied it to the The HI Nearby Galaxy Survey (THINGS) galaxy sample (Walter et al. 2008). Their analysis showed that H₂ plays a significant role in disc (in)stability by dynamically decoupling and dominating the onset for gravitational instability even at distances as large as half the optical radius.

The goal of this work is to in greater details explore the interplay between gas turbulence and disc stability by extending previous work in a number of ways.

(i) We perform numerical simulations of a Milky Way-like galaxy with a resolution of ~ 9 pc, where we model the same galaxy in two markedly different ways: (1) without any stellar feedback, leading to rapid gas fragmentation into a population of star-forming GMCs, and (2) with efficient stellar feedback which acts to disperse the GMCs, drives interstellar turbulence, and regulates the rate of star formation. These two models show two extremes of galaxy evolution, and are useful platforms on which to understand, and characterize, the role of turbulence in realistic disc galaxies.

(ii) We apply a classical stability analysis on kpc-scales to both models and demonstrate how it fails to qualitatively separate the two systems, despite the dramatically different ISM morphology.

We show that this is in agreement with observations of nearby spiral galaxies.

(iii) By accounting for the scale-dependent nature of Σ and σ in a multicomponent stability analysis, we demonstrate how we can more robustly characterize the disc stability and dynamical state of the galaxies.

The rest of the paper is organized as follows. The classical framework for understanding the stability of two-component thick discs is outlined in Sections 2.1 and 2.2. In Section 2.3, we describe the numerical hydro+N-body method used for the galaxy simulations. In Section 3.1, we perform a classical analysis followed by an accounting of turbulent scaling relations in Section 3.2. In Section 3.3, we discuss our results in a more general context of observed, and theoretically predicted, ISM scaling relations and what this means for understanding disc galaxies. Finally, we discuss and conclude our results in Section 4.

2 METHOD

2.1 Stability diagnostics

Consider a gas disc of scaleheight h , and perturb it with axisymmetric waves of frequency ω and wavenumber k . The response of the disc is described by the dispersion relation

$$\omega^2 = \kappa^2 - \frac{2\pi G \Sigma k}{1 + kh} + \sigma^2 k^2, \quad (2)$$

where κ is the epicyclic frequency, Σ is the surface density at equilibrium, and σ is the sound speed (Romeo 1992, 1994, see also Vandervoort 1970). The three terms on the right-hand side of equation (2) represent the contributions of rotation, self-gravity, and pressure. For $kh \ll 1$, equation (1) reduces to the usual dispersion relation for an infinitesimally thin gas disc (for a derivation, see e.g. Binney & Tremaine 2008). Such a disc is unstable if and only if $\omega^2 < 0$, which is equivalent to $Q < 1$, where Q is defined by

$$Q = \frac{\kappa \sigma}{\pi G \Sigma}. \quad (3)$$

This quantity was first derived by Toomre (1964) for a thin disc of stars (where $\sigma \rightarrow \sigma_R$, i.e. the stellar radial velocity dispersion, and the denominator has π replaced by 3.36), and we hence refer to it as Toomre's Q . From now on, we denote equation (3) for stars and gas as Q_* and Q_g , respectively. For $kh \gg 1$, one recovers the case of Jeans instability with rotation, since $\Sigma/h \approx 2\rho$. In other words, scales comparable to h mark the transition from 2D to 3D stability.

Much work has gone into characterizing gravitational instabilities in multicomponent systems (Bertin & Romeo 1988; Romeo 1992, 1994; Elmegreen 1995; Jog 1996; Rafikov 2001). Such systems are always more unstable than each component considered separately, and the interplay between the different components depends on the ratio between their velocity dispersions and their surface densities. Romeo & Wiegert (2011) introduced a simple and accurate approximation for the two-component Q parameter, which takes into account the stabilizing effect of disc thickness and predicts whether the local stability level is dominated by stars or gas. Romeo & Falstad (2013) generalized this approximation to discs made of several stellar and/or gaseous components, and to the whole range of velocity dispersion anisotropies observed in galactic discs. In the

two-component case, the Q stability parameter is given by

$$\frac{1}{Q_{\text{thick}}} = \begin{cases} \frac{W}{T_* Q_*} + \frac{1}{T_g Q_g} & \text{if } T_* Q_* \geq T_g Q_g, \\ \frac{1}{T_* Q_*} + \frac{W}{T_g Q_g} & \text{if } T_g Q_g \geq T_* Q_*; \end{cases} \quad (4)$$

$$W = \frac{2\sigma_*\sigma_g}{\sigma_*^2 + \sigma_g^2}. \quad (5)$$

$$T \approx \begin{cases} 1 + 0.6 \left(\frac{\sigma_z}{\sigma_R} \right)^2 & \text{for } 0 \lesssim \sigma_z/\sigma_R \lesssim 0.5, \\ 0.8 + 0.7 \left(\frac{\sigma_z}{\sigma_R} \right) & \text{for } 0.5 \lesssim \sigma_z/\sigma_R \lesssim 1. \end{cases} \quad (6)$$

The thin-disc limit, Q_{thin} , can be recovered by setting $\sigma_z/\sigma_R = 0$ and hence $T = 1$. As for the single-component case, the criterion for instability is $Q_{\text{thick}} < 1$ and $Q_{\text{thin}} < 1$.

2.2 Accounting for turbulent scalings

As discussed in Section 1, observations and theory have revealed that the ISM is highly turbulent, and many properties of the ISM depend on the physical scale on which they are measured. As argued by Romeo, Burkert & Agertz (2010), turbulence can be accounted for in the stability diagnostics by generalizing the dispersion relation in equation (2) to account for scale dependences of the velocity dispersion σ and surface density Σ , i.e.

$$\omega^2 = \kappa^2 - 2\pi G \Sigma(k) k + \sigma^2(k) k^2, \quad (7)$$

where $\Sigma(k)$ and $\sigma(k)$ are the mass column density and the 1D velocity dispersion (accounting both for the thermal and turbulent component) measured over a region of size $\ell = 2\pi/k$. Observations and theoretical studies (see e.g. Larson 1981; Elmegreen & Scalo 2004; Kritsuk et al. 2007; McKee & Ostriker 2007; Romeo et al. 2010) indicate a power-law behaviour in these quantities, motivating the following parametrization:

$$\Sigma(k) = \Sigma_0 \left(\frac{k}{k_0} \right)^{-a}, \quad \sigma(k) = \sigma_0 \left(\frac{k}{k_0} \right)^{-b}. \quad (8)$$

If the disc has volume density ρ and scaleheight h , then $\Sigma \approx 2\rho\ell$ for $\ell \lesssim h$ and $\Sigma \approx 2\rho h$ for $\ell \gtrsim h$. The range $\ell \lesssim h$ corresponds to the case of 3D turbulence (relevant for GMCs and H I on small scales), whereas the range $\ell \gtrsim h$ corresponds to the case of 2D turbulence (relevant for H I on large scales). The quantity $\ell_0 = 2\pi/k_0$ is the typical scale at which Σ and σ are observed and quantities like the Toomre parameter Q is computed, so that $Q_0 = \kappa\sigma_0/\pi G\Sigma_0$. For example, at an angular resolution of 6 arcsec achieved for the THINGS galaxy sample (Walter et al. 2008), analysis is carried out on the spatial smoothing scale $\ell_0 \sim 0.5 - 1$ kpc (Leroy et al. 2008).

As we are interested in understanding the influence of turbulence on a two-component disc (gas and stars), we need to analyse the joint dispersion relation which can then be expressed in the following form (e.g. Jog & Solomon 1984; Hoffmann & Romeo 2012):

$$(\omega^2 - \mathcal{M}_1^2)(\omega^2 - \mathcal{M}_2^2) = (\mathcal{P}_1^2 - \mathcal{M}_1^2)(\mathcal{P}_2^2 - \mathcal{M}_2^2), \quad (9)$$

where the (turbulent) dispersion relation for each component i has the usual form

$$\mathcal{M}_i^2 \equiv \kappa^2 - 2\pi\pi G \Sigma_i(k) k + \sigma_i^2(k) k^2, \quad (10)$$

and

$$\mathcal{P}_i^2 \equiv \kappa^2 + \sigma_i^2(k) k^2, \quad (11)$$

with $i = \text{gas, star}$.² Note that $\mathcal{M}_i^2(k)$ is the one-component dispersion relation for potential-density waves, while $\mathcal{P}_i^2(k)$ describes sound waves modified by rotation and turbulence. Furthermore, the right-hand side of equation (9) measures the strength of the gravitational coupling between the two components, as $\mathcal{M}_i^2(k) - \mathcal{P}_i^2(k)$ is the self-gravity term of component i . Equation (9) is quadratic in ω^2 , with two real roots:

$$\omega_{\pm}^2 = \frac{1}{2} \left[\mathcal{M}_1^2 + \mathcal{M}_2^2 \pm \sqrt{\Delta} \right], \quad (12)$$

$$\Delta = (\mathcal{M}_1^2 - \mathcal{M}_2^2)^2 + 4(\mathcal{P}_1^2 - \mathcal{M}_1^2)(\mathcal{P}_2^2 - \mathcal{M}_2^2). \quad (13)$$

This means that the dispersion relation has two branches that do not cross, $\omega_+^2(k) \neq \omega_-^2(k)$, except possibly as $k \rightarrow 0$ or $k \rightarrow \infty$. We focus only on $\omega_-^2(k)$ in this work, as this branch is the only one which can represent gravitational instability ($\omega_+^2(k)$ is manifestly ≥ 0). Note that $\omega_-^2(k)$ is always *smaller* than each component individually.

In Sections 3.2 and 3.3, we use the above framework, together with numerical simulations, to demonstrate how turbulence affects the shape of the dispersion relation, and hence the condition for local gravitational instability ($\omega^2 < 0$).

2.3 Numerical technique

In order to carry out hydro+ N -body simulations of galactic discs, we use the adaptive mesh refinement (AMR) code RAMSES (Teyssier 2002). The fluid dynamics of the baryons is calculated using a second-order unsplit Godunov method, while the collisionless dynamics of stellar and dark matter particles is evolved using the particle-mesh technique (Hockney & Eastwood 1981), with gravitational accelerations computed from the gravitational potential on the mesh. The gravitational potential is calculated by solving the Poisson equation using the multigrid method (Guillet & Teyssier 2011) for all refinement levels. The equation of state of the fluid is that of an ideal monoatomic gas with an adiabatic index $\gamma = 5/3$.

The code achieves high resolution in high-density regions using AMR, where the refinement strategy is based on a quasi-Lagrangian approach in which the number of collisionless particles per cell is kept approximately constant. This allows the local force softening to closely match the local mean interparticle separation, which suppresses discreteness effects (e.g. Romeo et al. 2008). An analogous refinement criterion is also used for the gas.

The star formation, cooling physics, and stellar feedback model adopted in our simulations is described in detail in Agertz et al. (2013, identical to the ‘A11’ model) and Agertz & Kravtsov (2014), and we refer the reader to those papers for details. Briefly, several processes contribute to the stellar feedback budget, as stars inject energy, momentum, mass, and heavy elements over time via SNII and SNIa explosions, stellar winds, and radiation pressure into the surrounding gas. Metals injected by supernovae and stellar winds are advected as a passive scalar and are incorporated self-consistently in the cooling and heating routine.

One aspect differs from previous work; at the current numerical resolution ($\Delta x \sim 9$ pc), we are not guaranteed to always resolve the

² The dispersion relation of an N -component turbulent disc is $\sum_{i=1}^N (\mathcal{M}_i^2 - \mathcal{P}_i^2) / (\omega^2 - \mathcal{P}_i^2) = 1$, as can be inferred from equation 22 of Rafikov (2001).

cooling radius³ r_{cool} , i.e. the SN bubble radius for which radiative losses are expected to be important for each discrete SN event, leading to an underestimation of the impact of SNe feedback. Instead of remedying this issue by solving two separate energy equations, one for the thermal energy and one for the feedback energy as in Agertz & Kravtsov (2014), we adopt the model recently suggested by Kim & Ostriker (2014, see also Gatto et al. 2014; Martizzi, Faucher-Giguère & Quataert 2014; Simpson et al. 2014). Here, an SN explosion resolved by at least three grid cells ($r_{\text{cool}} \geq 3\Delta x$) is initialized in the energy conserving phase by injecting the relevant energy (10^{51} erg per SN) into the nearest grid cell. If this criterion is not fulfilled, the SN is initialized in its momentum conserving phase, i.e. the momentum generated during the energy conserving Sedov–Taylor phase is injected into to the 26 cells surrounding a star particle.

Blondin et al. (1998) calculated the transition time from the energy-conserving phase to the phase of shell formation, at which the cooling time equals the age of the remnant ($t_{\text{cool}} = t_{\text{SN}}$), to be $\approx 2.9 \times 10^4 E_{51}^{4/17} n_0^{-9/17}$ yr, where n_0 is the ambient density and E_{51} the thermal energy in units of 10^{51} ergs. At this time, the momentum of the expanding shell is approximately

$$p_{\text{ST}} \approx 2.6 \times 10^5 E_{51}^{16/17} n_0^{-2/17} M_{\odot} \text{ km s}^{-1}. \quad (14)$$

For reasonable values of ambient densities, this is ~ 10 times greater than the initial ejecta momentum. Kim & Ostriker (2014) and Martizzi et al. (2014) have shown, using detailed simulations of SNe explosions, that equation (14) holds even for more realistic, clumpy, environments. We hence use this relation for the injected momentum per individual SN explosion when the cooling radius is not resolved.

2.3.1 Simulations

We model the non-linear evolution of an entire Milky Way-like galactic disc. This setup is now the standardized test for the AGORA code comparison project (Kim, Abel & Agertz 2014), and is a higher resolution version of the galaxy analysed in Agertz et al. (2013). Briefly, following Hernquist (1993) and Springel (2000, see also Springel, Di Matteo & Hernquist 2005), we create a particle distribution representing a late type, star-forming spiral galaxy embedded in an NFW dark matter halo (Navarro, Frenk & White 1996). The dark matter halo has a concentration parameter $c = 10$ and virial circular velocity, measured at the overdensity $200\rho_{\text{crit}}$, $v_{200} = 150 \text{ km s}^{-1}$, which translates to a halo virial mass $M_{200} = 1.1 \times 10^{12} M_{\odot}$. The total baryonic disc mass is $M_{\text{disc}} = 4.5 \times 10^{10} M_{\odot}$ with 20 per cent in gas. The bulge-to-disc mass ratio is $B/D = 0.1$. We assume exponential profiles for the stellar and gaseous components and adopt a disc scalelength $r_{\text{d}} = 3.4 \text{ kpc}$ and scaleheight $h = 0.1r_{\text{d}}$ for both. The bulge mass profile is that of Hernquist (1990) with scalelength $a = 0.1r_{\text{d}}$. The halo and stellar disc are represented by 10^6 particles each, and the bulge consists of 10^5 particles.

We initialize the gaseous disc analytically on the AMR grid assuming an exponential profile. The galaxy is embedded in a hot ($T = 10^6 \text{ K}$), tenuous ($n = 10^{-5} \text{ cm}^{-3}$) gas halo enriched to $Z = 10^{-2} Z_{\odot}$, while the disc has solar abundance. The minimum AMR cell size reached in the simulations is $\Delta x = 9 \text{ pc}$.

We carry out two simulations, one without any stellar feedback, adopting a local star formation efficiency per free-fall time (see e.g. Agertz et al. 2013) $\epsilon_{\text{ff}} = 1$ per cent, and one with stellar feedback but with $\epsilon_{\text{ff}} = 10$ per cent. In the former case, the effect of feedback is implicit in the choice of ϵ_{ff} , and in the latter case this is achieved by efficient stellar feedback. Both simulations therefore have similar star formation histories and normalizations of the $\Sigma_{\text{SFR}}-\Sigma_{\text{gas}}$ (Kennicutt–Schmidt) relation (see discussion in Agertz et al. 2013; Agertz & Kravtsov 2014), but reach this state in different ways.

3 RESULTS

3.1 Classical stability analysis

The left-hand side of Fig. 1 shows projected gas surface density maps of the two simulated galactic discs at $t = 140 \text{ Myr}$. Without stellar feedback, the disc violently fragments into a long-lived population of massive star-forming GMCs, whereas the clouds are rapidly dispersed, and reformed, in the feedback regulated case. In the right-hand panel, we show radial profiles of the classical Toomre Q for gas and stars, as well as the two-component thin and thick disc stability parameter, Q_{thin} and Q_{thick} , respectively (see Section 2.1).

We find all Q radial profiles to be almost indistinguishable between the two models, and note that they are in agreement with derived values from well-resolved spiral galaxies, see e.g. the detailed analysis by Leroy et al. (2008) of the THINGS galaxies (see also fig. 5 in Romeo & Wiegert 2011; Romeo & Falstad 2013); e.g. $Q_{\text{thick}} \sim 1.5\text{--}3$ for $r \gtrsim 2 \text{ kpc}$, i.e. outside the bulge, indicative of gravitational stability to axisymmetric waves. The similar values of $Q(r)$, all being significantly larger than unity, arise despite the morphological states of the discs being markedly different.

Leroy et al. (2008) concluded that the large observed values of Q , indicative of local stability,⁴ put doubts on the role of gravitational instabilities in *alone* controlling the local star formation efficiency. However, as we have been alluding to in previous sections, our analysis is done on a fixed, and rather large, scale ($\ell_0 = 0.5 \text{ kpc}$) chosen to coincide with the spatial resolution of the THINGS survey. The fact that different indicators of stability fail to separate the simulated galaxies means that galactic dynamics, on the chosen smoothing scale, is the same. To probe differences further, we need to adopt a scale-dependent stability analysis.

3.2 Accounting for turbulent scalings

In this section, we characterize the effect of turbulence on the gravitational stability of the simulated discs directly via the dispersion relation for gas and stars (equation 7), as well as the relation for the coupled system (ω_-^2 in equation 12).

We estimate $\Sigma(\ell)$ and $\sigma(\ell)$ for gas and stars from the simulations at different simulation times as follows; assume the disc plane coincides with the xy -plane, i.e. the axis of rotation is parallel with the z -axis. Centred in the mid-plane of the disc ($z = 0$), we place cubes in a lattice configuration in the range $(x, y) \in \{-15, 15\} \text{ kpc}$, with a lattice spacing of $\Delta l = 100 \text{ pc}$. Starting from a cube size of $\ell = 36 \text{ pc}$, we incrementally increase this value by $2\Delta x = 36 \text{ pc}$ up to $\ell = 0.5 \text{ kpc}$, after which we increase the cube sizes in steps of

³ The cooling radius scales as $r_{\text{cool}} \approx 30n_0^{-0.43}(Z/Z_{\odot} + 0.01)^{-0.18} \text{ pc}$ for a supernova explosion with energy $E_{\text{SN}} = 10^{51} \text{ erg}$ (e.g. Cioffi, McKee & Bertschinger 1988; Thornton et al. 1998; Kim & Ostriker 2014).

⁴ Note that this refers to stability against axisymmetric perturbations and that stability against *non*-axisymmetric perturbations is not guaranteed (e.g. Griv & Gedalin 2012).

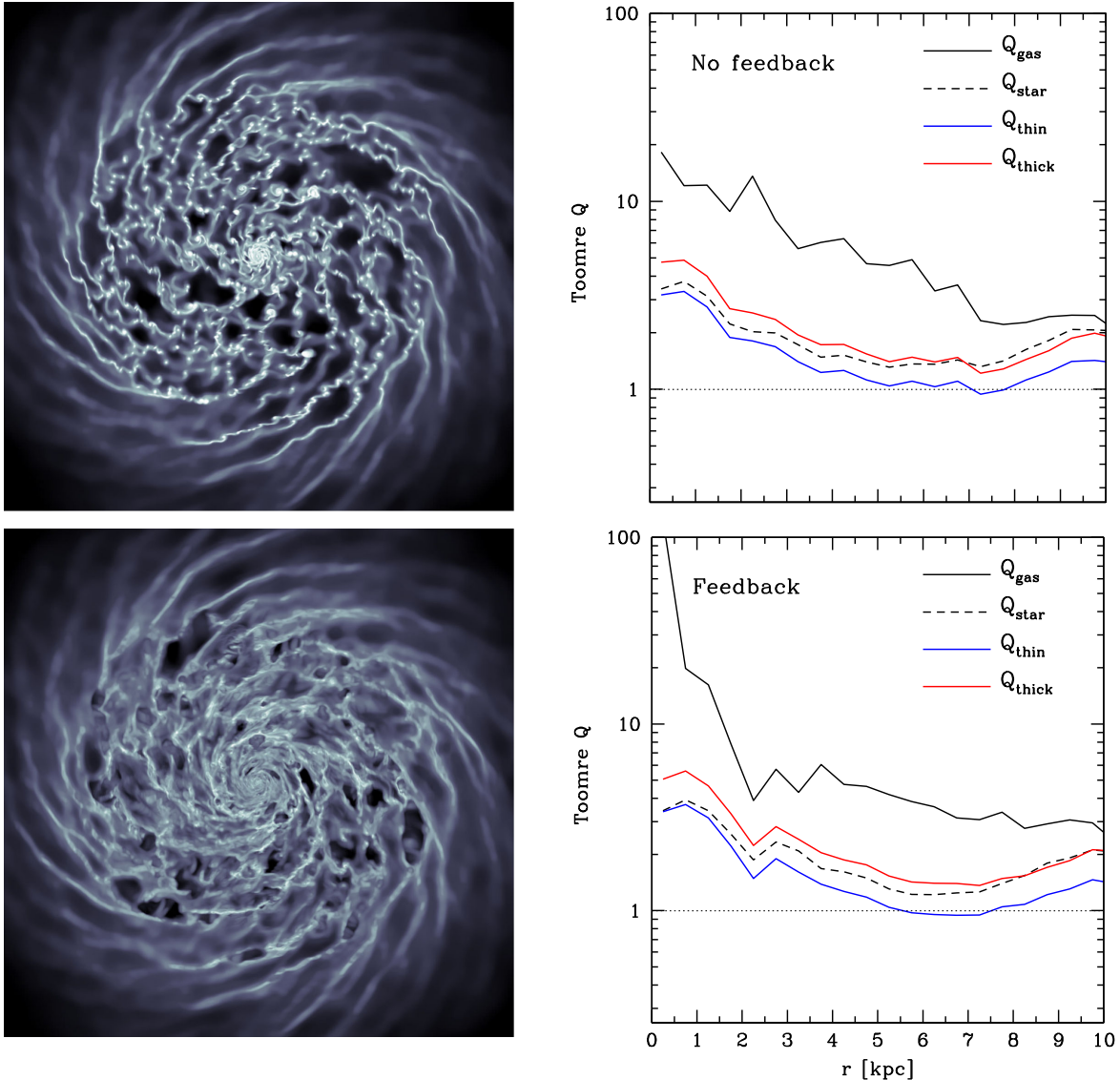


Figure 1. (Left) Projected gas density maps covering a region $36 \text{ kpc} \times 36 \text{ kpc}$ in size at $t = 140 \text{ Myr}$ of the simulation without (top) and with (bottom) stellar feedback. (Right) Mass-weighted average profiles, computed in radial bins of size $\Delta r = 0.5 \text{ kpc}$ of the classical Toomre Q ($= \sigma \kappa / \pi G \Sigma$) for gas and stars, the joint stability parameter Q_{thin} , and the joint parameter accounting for disc thickness Q_{thick} (Romeo & Wiegert 2011; Romeo & Falstad 2013).

50 percent of the current value up to $\ell \sim 10 \text{ kpc}$, simply to reduce the computational cost. On each scale, we compute $\Sigma_i(\ell)$ and $\sigma_i(\ell)$ for each component (gas and stars) for every cube i . We then define $\Sigma(\ell)$ and $\sigma(\ell)$ to be the averages of all cubes at any given scale, and consider these quantities to be representative of the typical surface density and velocity dispersion. We have confirmed that sampling the discs in different way, e.g. randomly, has a negligible effect on the results presented below.

From now on, we focus our analysis on the average scale-dependent characteristics centred in an azimuth defined by $4 \text{ kpc} < r < 5 \text{ kpc}$. Furthermore, as the gaseous velocity dispersion is found not to be isotropic (see also discussion in Agertz et al. 2009a), we will from here on consider the radial velocity dispersion $\sigma_R(\ell)$ for both gas and stars, as this is the relevant component entering the dispersion relation for non-isotropic velocity ellipsoids. Note also that the sound speed of the gas $c_s \ll \sigma_R$ in a mass-weighted sense;

the cold ISM is dominated by supersonic motions, and we can in principle omit c_s in the stability analysis.

3.2.1 Density evolution and spatial scaling

Fig. 2 shows the time evolution ($t = 60, 100$, and 140 Myr) of $\Sigma_{\text{gas}}(\ell)$ and $\Sigma_{\text{star}}(\ell)$ for the fragmenting (no feedback) and feedback-regulated discs. Both simulations show ‘saturated’ quantities above $\ell \sim 1 \text{ kpc}$, above which little variation with scale is found, confirming the strikingly similar $Q(r)$ values found in Section 3.1. On smaller scales, the two models evolve differently; without feedback at $t = 140 \text{ Myr}$ (and as well for earlier times, but on scales of a few 100 pc), the population of bound star-forming clouds, arising from violent fragmentation, leads to a steeply decreasing $\Sigma_{\text{gas}}(\ell)$ with increasing ℓ , while the feedback regulated case shows a rather flat $\Sigma_{\text{gas}}(\ell)$. Quantified using the power-law relation in equation (8)

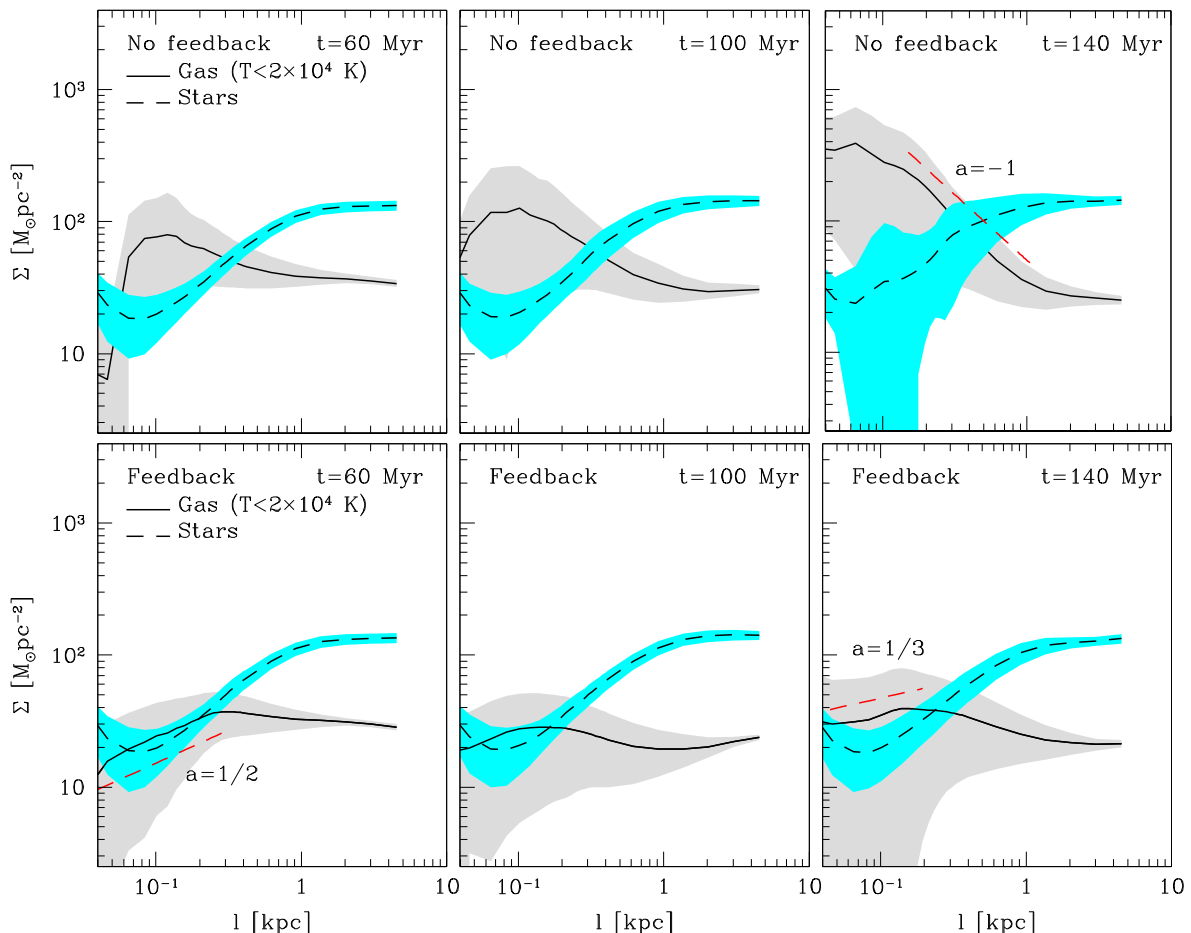


Figure 2. The scale dependence of the gas and stellar surface density Σ in the models adopting no feedback (top) and feedback (bottom) for, from left to right, $t = 60, 100,$ and 140 Myr.

($\Sigma \propto \ell^a$), the clumpy galaxy approaches $a \sim -1$ and the feedback-regulated $a \sim 0$ for $\ell \lesssim 1$ kpc. Significant scatter exists in the data, owing to the structured nature of the ISM and the fact that we do not bias the analysis to any specific regions of the disc⁵ or phases of the gas, other than the cold ISM.

$\Sigma_{\text{star}}(\ell)$ is increasing at scales larger than ~ 100 pc. This is due to the analysis being done in mid-plane-centred cubes, for which scales $\ell \sim 1$ kpc do not encapsulate all of the (kinematically hot) stars present in the disc. A similar conclusion may be drawn for the cold gas in the feedback-regulated simulation, where the small-scale turbulence, in an average sense, allows for a positive value of a . Adopting a scale-dependent analysis for both stars and gas hence automatically accounts for disc thickness, without the need to adopt an effective surface density $\Sigma_{\text{eff}} = \Sigma/(1 + kh)$, as is done in equation (2).

3.2.2 Velocity dispersion evolution and spatial scaling

Fig. 3 shows the time evolution, $t = 60, 100,$ and 140 Myr, of $\sigma_{\text{R,star}}(\ell)$ and $\sigma_{\text{R,gas}}(\ell)$ for the fragmenting (no feedback)

and feedback-regulated discs. The stars show a roughly scale-independent value of $\sigma_{\text{R}} \sim 30 \text{ km s}^{-1}$ in both disc models. For the cold gas, we find that the velocity dispersions are, after an initial transient, quite similar both in magnitude and dependence on scale regardless of the presence of feedback or not. In both models, and for $t > 60$ Myr, $\sigma_{\text{R,gas}}(\ell) \propto \ell^{1/2}$ on scales $\ell \lesssim 300\text{--}400$ pc in the feedback model, and $\ell \lesssim 100$ pc in the model without, in excellent agreement with the observed Larson-like scaling relevant for GMCs (see Section 1).

Still at times $t > 60$ Myr, and on large scales (a few $100 \text{ pc} \lesssim \ell \lesssim 4$ kpc), the slope of $\sigma_{\text{R,gas}}(\ell)$ transitions from $b \sim 1/2$, into a flatter profile, with $b \sim 1/5$, in the case without feedback. In the feedback-regulated galaxy, we measure $b \sim 1/2$ up to almost ~ 1 kpc, with a flattening on scales $\gtrsim 1$ kpc. The slopes, and the scales over which the relation is measured in the feedback model, are in excellent agreement with observations of the Galactic H I line-width–scale relation. For example, Kim et al. (2007) studied this relation for individual H I clouds in the Large Magellanic Cloud and found $b \sim 0.3\text{--}0.5$ on scales $\lesssim 0.5\text{--}1$ kpc (down to parsec scales).

We emphasize that both models show values of $\sigma \sim 10\text{--}20 \text{ km s}^{-1}$ on large scales, in agreement with both H I and CO observations in local spiral galaxies (Tamburro et al. 2009; Caldú-Primo et al. 2013), despite the different nature in ISM turbulence driving on small scales. In the case of feedback-driven turbulence, star-forming clouds are rapidly destroyed by internal process and the gas is dispersed, whereas disordered gas motions are driven

⁵ For example, by not enforcing the analysis to be centred *only* on the dense cloud population in the fragmented disc, we do not measure a monotonically increasing $\Sigma(\ell)$ as $\ell \rightarrow 0$.

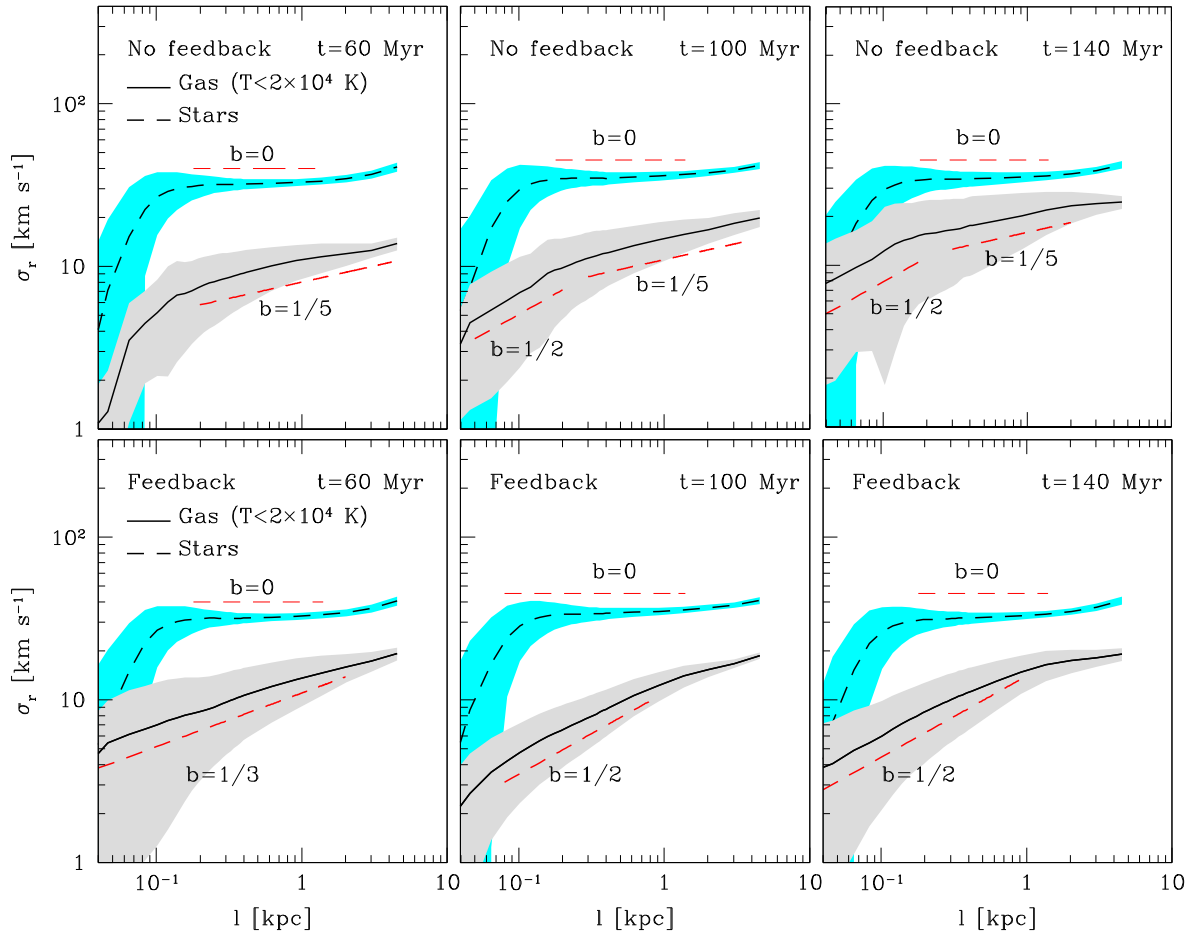


Figure 3. The scale dependence of the gas and stellar radial velocity dispersion σ_r in the models adopting no feedback (top) and feedback (bottom) for, from left to right, $t = 60, 100,$ and 140 Myr.

by gravitational instabilities and galactic shear, leading to clump-clump interactions (e.g. Jog & Ostriker 1988; Gammie, Ostriker & Jog 1991; Agertz et al. 2009a; Tasker & Tan 2009) in the case without feedback.

3.2.3 The dispersion relation

Fig. 4 shows the resulting mass-weighted average dispersion relations, and the associated scatter, for the two galactic models for the stars (ω_{stars}^2), cold gas (ω_{gas}^2), and the coupled system (ω^2). We remind the reader that the average $\omega^2(\ell)$ relations now self-consistently account for the actual scale-dependent values of $\sigma(\ell)$ and $\Sigma(\ell)$ present in each analysed region of the galaxies.

While featuring an almost identical $Q(r)$ (for $t = 140$ Myr, Section 3.1), when analysed on ~ 1 kpc scales, we can here identify the level of stability on all scales. Both discs are indeed stable or marginally stable ($\omega^2 \geq 0$) on large scales, and have in fact almost identical $\omega^2(\ell)$ relations for $\ell \gtrsim 1$ kpc.

The fragmented disc without stellar feedback always shows $\omega_{\text{gas}}^2 < 0$ and $\omega^2 < 0$ on small scales, as suspected simply via visual inspection of the top-left panel of Fig. 1. At early times ($t = 60$ Myr), when fragmentation has just occurred, the scale of instability is formally as large as ~ 2 kpc, with scales below a few ~ 100 pc being the most unstable. At subsequent times, $\omega^2 < 0$ on scales $\ell \lesssim 100 - 200$ pc, roughly the maximum size of GMCs, or more correctly GMAs (Giant Molecular Associations) in this

model. This is also the scale at which we measured a transition in the Larson-like scaling of the gas velocity dispersions, from $b \sim 1/2$ into $b \sim 1/5$ (Section 3.2.2).

The above conclusions are in stark contrast to the feedback-regulated case which is, at least on average, stable or marginally stable on all scales. Note that individual patches of the disc on small scales can be unstable, leading to star formation, as is evident for $\omega_{\text{gas}}^2(\ell \lesssim 100 \text{ pc})$ at a $\gtrsim 0.5 \sigma$ level.

This analysis underscores the necessity to extend a traditional stability analysis with scale-dependent variables to account for the typical average velocity and density structures that exists in the ISM. Furthermore, many classical concepts, such as a well-defined fastest growing mode for a Toomre unstable ($Q < 1$) disc, may no longer exist for the emerging scalings of $\Sigma(\ell)$ and $\sigma(\ell)$ introduced by strong fragmentation, as pointed out by Romeo et al. (2010) and Romeo & Agertz (2014).

3.3 Mapping out the stability regimes

How do the results in the previous sections connect to observed turbulent scaling in the ISM and results from high-resolution numerical simulations? Fig. 5 shows the *stability map of turbulence* (Romeo et al. 2010), where the axes denote the a and b power-law exponents for the surface density and the velocity dispersion (equation 8).

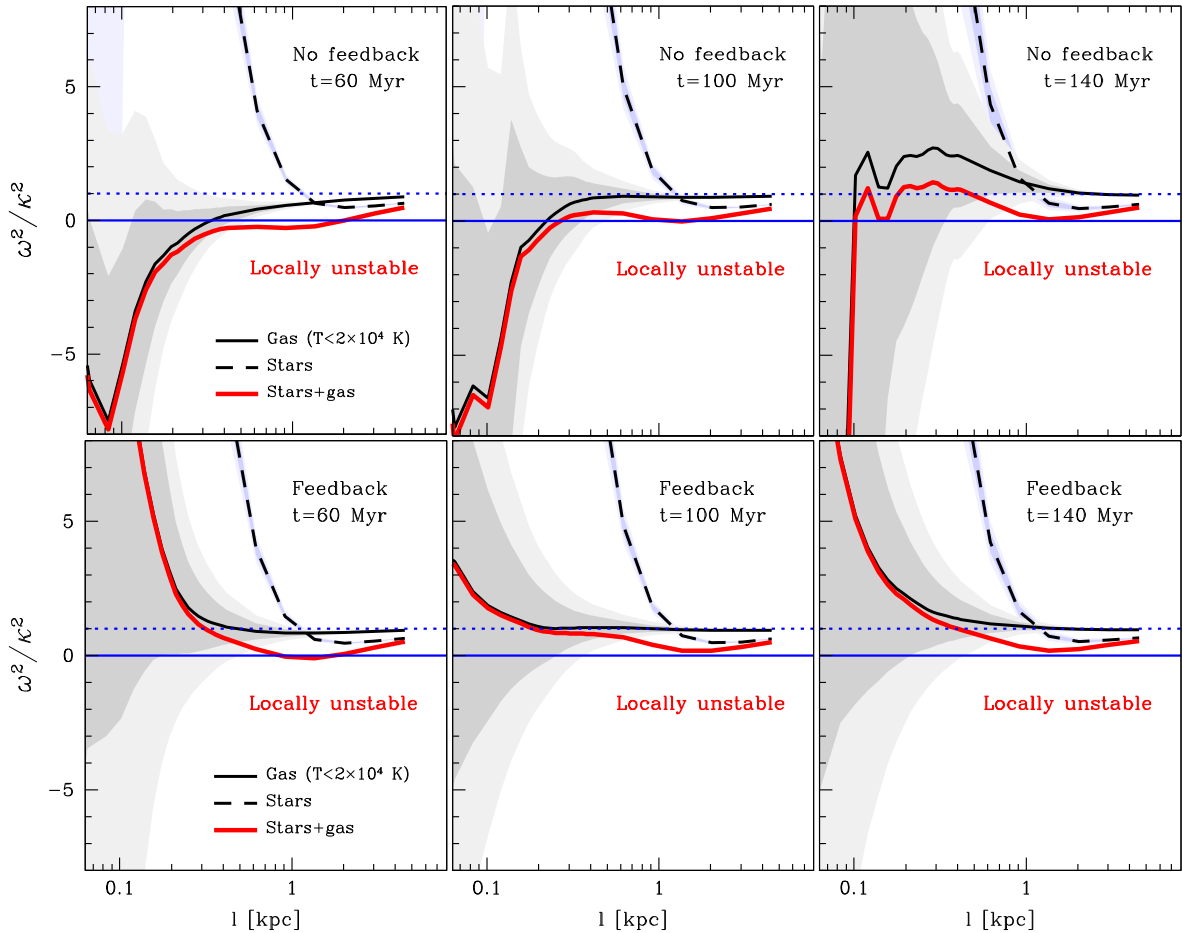


Figure 4. The instability growth rate, accounting for scale-dependent $\sigma(\ell)$ and $\Sigma(\ell)$, for gas (solid lines) and stars (dashed lines) for no feedback (top) and feedback (bottom). When turbulent scalings are accounted for in the analysis, the feedback simulation is found to be on average stable on all scales, with a Toomre-like behaviour (see main text), whereas the model lacking feedback is characterized as unstable on small scales ($\ell \lesssim$ a few 100 pc), in accordance with the fragmented gas morphology with star forming clouds of sizes ~ 100 pc.

Following the analysis in Romeo et al. (2010, see also Hoffmann & Romeo 2012), we have identified, and indicated in the figure, three regimes of stability.

(i) *Regime A*: for $b < \frac{1}{2}(1+a)$ and $-2 < a < 1$, the stability of the disc is controlled by $Q_0 = \kappa\sigma_0/\pi G\Sigma_0$ (i.e. the Q measured on the fiducial smoothing scale ℓ_0 , see Section 2.2): the disc is stable at all scales if and only if $Q_0 \geq \bar{Q}_0$, where \bar{Q}_0 depends on a , b , and ℓ_0 , and must be derived from equation (7) for a single-component system. This is the domain of H I turbulence. Both H I observations and high-resolution simulations of supersonic turbulence are consistent with the scaling $a \sim b$. In the case when $a = b$, the ratio $\sigma(\ell)/\Sigma(\ell)$ is a constant and the local stability criterion degenerates into the classical Toomre case, $Q_0 \geq 1$, as if the disc was non-turbulent and infinitesimally thin.

(ii) *Regime C*: for $b > \frac{1}{2}(1+a)$ and $-2 < a < 1$, the stability of the disc is no longer controlled by Q_0 : the disc is always unstable on small scales (i.e. as $l \rightarrow 0$) and stable on large scales.

(iii) *Regime B*: for $b = \frac{1}{2}(1+a)$ and $-2 < a < 1$, the disc is in a phase of transition between Toomre-like stability (Regime A) and instability on small scales (Regime C). This is the domain typically observed for molecular gas in GMCs.

A few well-studied examples from theory/simulations and observations in the literature are shown in the figure.

(i) (L), $(a, b) = (-0.1, 0.38)$: the original scaling relations in GMCs found by Larson (1981).

(ii) (S), $(a, b) = (0, 0.50 \pm 0.05)$: the scaling relations in GMCs found by Solomon et al. (1987). These values are what is usually referred to as ‘Larson’s scaling laws’.

(iii) (K), $(a, b) = (\frac{1}{3}, \frac{1}{2})$: the result of high-resolution simulations of supersonic turbulence (Kritsuk et al. 2013, Kritsuk, private communication).

(iv) (F), $(a, b) = (0.44 \pm 0.14, 0.49 \pm 0.02)$: a prediction based on state-of-the-art simulations of supersonic turbulence with compressive driving (Federrath 2013, Federrath, private communication). For solenoidal driving, $(a, b) = (0.58 \pm 0.03, 0.48 \pm 0.02)$.

(v) (E), $(a, b) = (-1, 0.5)$: investigated by Elmegreen (1996)

(vi) (H I): typical range of values derived from observed H I intensity fluctuations in disc galaxies (Lazarian & Pogosyan 2000; Kim et al. 2007; Roy et al. 2008).

A number of typical (a, b) pairs measured in the two simulations are indicated in Fig. 5. In the case of no feedback, leading to strong fragmentation, the disc features $a \sim -1$ to 0, and $b \sim 1/5 - 1/2$ on small/intermediate scales. This puts the disc in regime B and C, with the latter meaning that the disc is always unstable on small scales. In fact, by studying the dispersion relations ($\omega_{\text{gas}}^2(\ell)$ or $\omega^2(\ell)$) in Fig. 4, no well-defined minimum exists, with the smallest numerically resolved scale, here of the order of a cell size $\sim \Delta x$, being the

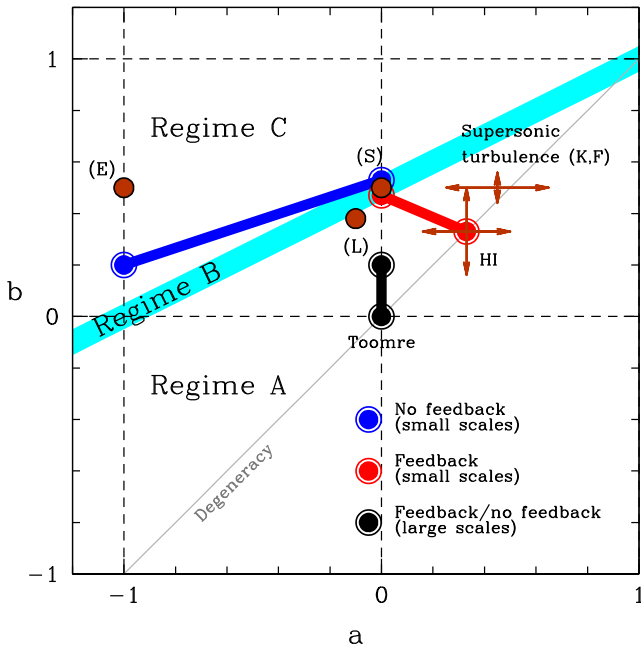


Figure 5. The stability map of turbulence, with typical values derived from observations and numerical simulations, see the main text for a comprehensive discussion. The blue, red, and black points indicate the regimes found in the simulated disc galaxies on both small and large scales. On large scales ($\ell \gtrsim 1$ kpc), the feedback-regulated disc and the fragmented disc converge to roughly the same average Σ and σ , and both well described by a Toomre-like stability criterion (Regime A, see text). Turbulent scaling on small scales pushes the fragmented disc into a regime typical observed for GMCs (Regime B), and a regime where the classical Toomre analysis is no longer valid (Regime C). The disc with feedback-driven turbulence is, in a statistical sense, stabilized on small scales, and shows scalings in broad agreement with H I and CO observations.

fastest growing mode. On large scales, we measure a transition into Regime A with $(a, b) \sim (0, 0)$, i.e. the classical Toomre case with a well-defined average surface density and velocity dispersion.

The feedback-driven simulation shows the same behaviour on large scales ($\ell \gtrsim 1$ kpc) as the fragmented counterpart, coinciding with the classical Toomre case. On small scales ($\ell \lesssim 1$ kpc), the simulations diverge, as discussed already in Section 3.2.3. Here, feedback creates an, on average, marginally stable ISM, still in regime A, with a and b values compatible with observations of the cold galactic ISM (H I and CO). Using these power-law exponents, one can define a Q stability parameter from equations (7) or (12) that quantifies the threshold for instability, in contrast to the case where the disc fragments due to the lack of stellar feedback support.

4 DISCUSSION AND CONCLUSIONS

Gravitational instabilities are thought to play an important role in galaxy evolution and star formation. In this work, we have investigated, using numerical simulations of Milky Way-like disc galaxies, the nature of turbulence in the ISM and how this affects the gravitational stability of galaxies. Clumpy/turbulent discs are dynamically similar to gas discs with scale-dependent surface densities and velocity dispersions, i.e. $\Sigma(\ell) \sim \ell^a$ and $\sigma(\ell) \sim \ell^b$, respectively, where ℓ is the physical scale. By taking these ‘turbulent’ scaling relations into account in the disc stability analysis, a wide variety of non-classical stability properties arise (Romeo et al. 2010).

In order to quantify the kind of turbulent scaling that develop in the ISM of disc galaxies, we used numerical simulations of multicomponent, Milky Way-like, galactic discs. We studied two markedly different evolutionary scenarios using the same initial condition: (1) no stellar feedback, leading to complete disc fragmentation and (2) efficient stellar feedback leading to driven ISM turbulence. By accounting for the measured turbulent scalings in the stability analysis, we could more robustly characterize the level stability as a function of physical scale. Our key results are summarized below.

(i) Our two different models of galaxy evolution lead to discs with nearly identical stability properties when quantified on kpc-scales by the classical Toomre Q for stars and gas separately ($Q \gg 1$), as well as jointly ($Q_{\text{stars+gas}} > 1$, accounting for disc thickness); the discs are stable at all radii. This notion is in good agreement with observations of nearby disc galaxies, e.g. THINGS (Leroy et al. 2008) where all discs, smoothed on kpc scales, featured values of Q_{gas} and Q_* well above unity (see also Romeo & Wiegert 2011), raising doubts on the role of gravitational instabilities in star formation.

(ii) The two models feature markedly different average $\Sigma(\ell)$ on scales $\ell < 1$ kpc, with a steepening of $\Sigma(\ell)$ into $\sim \ell^{-1}$ in the fragmented disc and $\sim \ell^{-1/3}$ for the feedback-regulated disc. Less of a difference was found for $\sigma(\ell)$, with a Larson-like scaling ($\sigma(\ell) \sim \ell^{1/2}$; Larson 1981; Solomon et al. 1987) in both models.

(iii) Introducing scale-dependent variables in the multicomponent stability analysis leads to a more robust characterization of the level of instability. The feedback-driven model is, on average, stable or marginally stable on all scales, in contrast to the model without feedback, for which we can clearly identify the scales ($\ell \lesssim 100$ pc) where gravitational instability, leading to cloud formation, typically occurs. Large scales ($\ell \gtrsim 1$ kpc) show almost identical stability properties in both models, as the surface density and velocity dispersion ‘saturate’ into more well-defined, non-turbulent quantities, explaining the similarity between the markedly different ISM models when adopting a traditional large-scale stability analysis.

(iv) The disc stabilized by stellar feedback can still be, in a statistical sense, well described by a Toomre-like Q stability threshold. This is no longer true for the violently fragmenting disc, which enters a regime where a Q -like parameter loses its meaning and small scales are asymptotically more and more unstable, and stability can only occur on large scales (see also Romeo et al. 2010).

Hopkins & Christiansen (2013) investigated gravitational fragmentation in turbulent media, arguing that turbulent flows are always unstable on some scale, given enough time, as a broad spectrum of stochastic density fluctuations exists that can produce rare, but gravitationally unstable regions. This notion is compatible with our results; by defining the typical densities and velocities existing at some scale in a mass-weighted sense, we are biasing ourselves towards dense regions. This gives us the *typical* structures, by mass, that exists in the ISM. However, the scatter in the dispersion relation for the model with feedback-driven turbulence (Fig. 4) can be substantial on small scales at any time, due to the wide range of densities in supersonically turbulent flows (e.g. Padoan, Jones & Nordlund 1997; Mac Low & Klessen 2004; Kritsuk et al. 2007). This means parts of the disc will be unstable, although the corresponding mass in that component may not necessarily be dominant.

In this work, we have not only considered Milky Way-like galaxies, with gas fractions typical of $z = 0$ discs. In high-redshift counterparts, with gas fractions several times greater (Tacconi et al. 2010), turbulence may play an even greater role in shaping the ISM. Indeed, the observed high levels of turbulence (e.g. Förster Schreiber

et al. 2009) is thought to be responsible for the highly clumpy morphologies observed (e.g. Agertz et al. 2009b; Dekel et al. 2009; Elmegreen et al. 2009; Tacconi et al. 2010; Genzel et al. 2011; Romeo & Agertz 2014). Current astronomical facilities such as Atacama Large Millimeter/submillimeter Array (ALMA) can resolve the scaling properties of galactic turbulence in the cold molecular gas of high-redshift systems, hence revealing the interplay between gravitational instability and turbulence in more extreme environments.

It is important to consider the limitations and assumptions behind the analysis presented in this work. The dispersion relation (equations 2 and 7) is formally only describing stability against local axisymmetric perturbations, i.e. it assumes that $kR \gg 1$. This is the short-wavelength approximation and is satisfied in our work as we only carry out our analysis at $R = 4$ kpc, and with $k = 2\pi/\ell$ this holds on all scales we have considered. However, the assumption of axisymmetry is not true in general, and non-axisymmetric perturbations are thought to have a greater destabilizing effect, i.e. discs that are formally stable ($Q > 1$) can be locally unstable against such perturbations. Local non-axisymmetric stability criteria are far more complex than Toomre's criterion as they depend critically on how tightly wound the perturbations are, and any such criteria cannot, in general, be expressed in terms of a single parameter akin to Toomre's Q (e.g. Lau & Bertin 1978; Bertin et al. 1989; Jog 1992; Griv & Gedalin 2012). We leave an analysis accounting for more general perturbations for future work.

In future work (Grisdale et al. in preparation), we will extend the analysis presented in this paper to quantify the gravitational stability for different gas phases, regions of the disc, as a function of local turbulence driving strength etc., and how this connects to properties of observed galaxies.

ACKNOWLEDGEMENT

We thank the referee for constructive comments and suggestions.

REFERENCES

- Agertz O., Kravtsov A. V., 2014, preprint ([arXiv:1404.2613](https://arxiv.org/abs/1404.2613))
- Agertz O., Lake G., Teyssier R., Moore B., Mayer L., Romeo A. B., 2009a, MNRAS, 392, 294
- Agertz O., Teyssier R., Moore B., 2009b, MNRAS, 397, L64
- Agertz O., Kravtsov A. V., Leitner S. N., Gnedin N. Y., 2013, ApJ, 770, 25
- Ballesteros-Paredes J., Hartmann L. W., Vázquez-Semadeni E., Heitsch F., Zamora-Avilés M. A., 2011, MNRAS, 411, 65
- Beaumont C. N., Goodman A. A., Alves J. F., Lombardi M., Román-Zúñiga C. G., Kauffmann J., Lada C. J., 2012, MNRAS, 423, 2579
- Begelman M. C., Shlosman I., 2009, ApJ, 702, L5
- Begum A., Chengalur J. N., Bharadwaj S., 2006, MNRAS, 372, L33
- Bertin G., Romeo A. B., 1988, A&A, 195, 105
- Bertin G., Lin C. C., Lowe S. A., Thurstans R. P., 1989, ApJ, 338, 104
- Binney J., Tremaine S., 2008, Galactic Dynamics, 2nd edn. Princeton Univ. Press, Princeton, NJ
- Block D. L., Puerari I., Elmegreen B. G., Bournaud F., 2010, ApJ, 718, L1
- Blondin J. M., Wright E. B., Borkowski K. J., Reynolds S. P., 1998, ApJ, 500, 342
- Bolatto A. D., Leroy A. K., Rosolowsky E., Walter F., Blitz L., 2008, ApJ, 686, 948
- Bournaud F., Elmegreen B. G., 2009, ApJ, 694, L158
- Bournaud F., Elmegreen B. G., Teyssier R., Block D. L., Puerari I., 2010, MNRAS, 409, 1088
- Caldú-Primo A., Schruha A., Walter F., Leroy A., Sandstrom K., de Blok W. J. G., Ianjamasimanana R., Mogotsi K. M., 2013, AJ, 146, 150
- Cioffi D. F., McKee C. F., Bertschinger E., 1988, ApJ, 334, 252
- Collins D. C., Kritsuk A. G., Padoan P., Li H., Xu H., Ustyugov S. D., Norman M. L., 2012, ApJ, 750, 13
- Combes F. et al., 2012, A&A, 539, A67
- Dekel A., Sari R., Ceverino D., 2009, ApJ, 703, 785
- Dobbs C. L., 2015, MNRAS, 447, 3390
- Dutta P., Begum A., Bharadwaj S., Chengalur J. N., 2008, MNRAS, 384, L34
- Dutta P., Begum A., Bharadwaj S., Chengalur J. N., 2009, MNRAS, 397, L60
- Dutta P., Begum A., Bharadwaj S., Chengalur J. N., 2013, New Astron., 19, 89
- Elmegreen B. G., 1995, MNRAS, 275, 944
- Elmegreen B. G., 1996, in Block D. L., Greenberg J. M., eds, Astrophysics and Space Science Library, Vol. 209, New Extragalactic Perspectives in the New South Africa. Kluwer, Dordrecht, p. 467
- Elmegreen B. G., Scalo J., 2004, ARA&A, 42, 211
- Elmegreen B. G., Kim S., Staveley-Smith L., 2001, ApJ, 548, 749
- Elmegreen B. G., Elmegreen D. M., Fernandez M. X., Lemos J. J., 2009, ApJ, 692, 12
- Federrath C., 2013, MNRAS, 436, 1245
- Federrath C., Klessen R. S., 2012, ApJ, 761, 156
- Federrath C., Roman-Duval J., Klessen R. S., Schmidt W., Mac Low M. M., 2010, A&A, 512, A81
- Fleck R. C., Jr, 1996, ApJ, 458, 739
- Förster Schreiber N. M. et al., 2009, ApJ, 706, 1364
- Fujimoto Y., Tasker E. J., Wakayama M., Habe A., 2014, MNRAS, 439, 936
- Gammie C. F., Ostriker J. P., Jog C. J., 1991, ApJ, 378, 565
- Gatto A. et al., 2014, preprint ([arXiv:1411.0009](https://arxiv.org/abs/1411.0009))
- Genzel R. et al., 2011, ApJ, 733, 101
- Griv E., Gedalin M., 2012, MNRAS, 422, 600
- Guillet T., Teyssier R., 2011, J. Comput. Phys., 230, 4756
- Hernquist L., 1990, ApJ, 356, 359
- Hernquist L., 1993, ApJS, 86, 389
- Heyer M., Krawczyk C., Duval J., Jackson J. M., 2009, ApJ, 699, 1092
- Hockney R. W., Eastwood J. W., 1981, Computer Simulation Using Particles. McGraw-Hill, New York
- Hoffmann V., Romeo A. B., 2012, MNRAS, 425, 1511
- Hopkins P. F., 2012, MNRAS, 423, 2016
- Hopkins P. F., Christiansen J. L., 2013, ApJ, 776, 48
- Hopkins P. F., Quataert E., Murray N., 2012, MNRAS, 421, 3488
- Hughes A. et al., 2010, MNRAS, 406, 2065
- Jog C. J., 1992, ApJ, 390, 378
- Jog C. J., 1996, MNRAS, 278, 209
- Jog C. J., Ostriker J. P., 1988, ApJ, 328, 404
- Jog C. J., Solomon P. M., 1984, ApJ, 276, 114
- Kauffmann J., Pillai T., Shetty R., Myers P. C., Goodman A. A., 2010, ApJ, 716, 433
- Kim J.-h. et al., 2014, ApJS, 210, 14
- Kim C. G., Ostriker E. C., 2014, preprint ([arXiv:1410.1537](https://arxiv.org/abs/1410.1537))
- Kim S. et al., 2007, ApJS, 171, 419
- Kowal G., Lazarian A., 2007, ApJ, 666, L69
- Kritsuk A. G., Norman M. L., Padoan P., Wagner R., 2007, ApJ, 665, 416
- Kritsuk A. G., Lee C. T., Norman M. L., 2013, MNRAS, 436, 3247
- Larson R. B., 1981, MNRAS, 194, 809
- Lau Y. Y., Bertin G., 1978, ApJ, 226, 508
- Lazarian A., Pogosyan D., 2000, ApJ, 537, 720
- Leroy A. K., Walter F., Brinks E., Bigiel F., de Blok W. J. G., Madore B., Thornley M. D., 2008, AJ, 136, 2782
- Lin C. C., Shu F. H., 1966, Proc. Natl. Acad. Sci., 55, 229
- Lombardi M., Lada C. J., Alves J., 2010, A&A, 512, A67
- McKee C. F., Ostriker E. C., 2007, ARA&A, 45, 565
- Mac Low M. M., Klessen R. S., 2004, Rev. Mod. Phys., 76, 125
- Martizzi D., Faucher-Giguère C. A., Quataert E., 2014, preprint ([arXiv:1409.4425](https://arxiv.org/abs/1409.4425))
- Navarro J. F., Frenk C. S., White S. D. M., 1996, ApJ, 462, 563
- Padoan P., Nordlund Å., 2011, ApJ, 730, 40
- Padoan P., Jones B. J. T., Nordlund A. P., 1997, ApJ, 474, 730
- Price D. J., Federrath C., 2010, MNRAS, 406, 1659

- Rafikov R. R., 2001, MNRAS, 323, 445
Renaud F. et al., 2013, MNRAS, 436, 1836
Roman-Duval J., Jackson J. M., Heyer M., Rathborne J., Simon R., 2010, ApJ, 723, 492
Romeo A. B., 1992, MNRAS, 256, 307
Romeo A. B., 1994, A&A, 286, 799
Romeo A. B., Agertz O., 2014, MNRAS, 442, 1230
Romeo A. B., Falstad N., 2013, MNRAS, 433, 1389
Romeo A. B., Wiegert J., 2011, MNRAS, 416, 1191
Romeo A. B., Agertz O., Moore B., Stadel J., 2008, ApJ, 686, 1
Romeo A. B., Burkert A., Agertz O., 2010, MNRAS, 407, 1223
Roy N., Peedikakkandy L., Chengalur J. N., 2008, MNRAS, 387, L18
Sánchez N., Añez N., Alfaro E. J., Crone Odekon M., 2010, ApJ, 720, 541
Schmidt W., Federrath C., Klessen R., 2008, Phys. Rev. Lett., 101, 194505
Shadmehri M., Khajenabi F., 2012, MNRAS, 421, 841
Shapiro K. L. et al., 2008, ApJ, 682, 231
Simpson C. M., Bryan G. L., Hummels C., Ostriker J. P., 2014, preprint (arXiv:1410.3822)
Solomon P. M., Rivolo A. R., Barrett J., Yahil A., 1987, ApJ, 319, 730
Springel V., 2000, MNRAS, 312, 859
Springel V., Di Matteo T., Hernquist L., 2005, MNRAS, 361, 776
Stanimirovic S., Staveley-Smith L., Dickey J. M., Sault R. J., Snowden S. L., 1999, MNRAS, 302, 417
Swinbank A. M. et al., 2011, ApJ, 742, 11
Tacconi L. J. et al., 2010, Nature, 463, 781
Tamburro D., Rix H. W., Leroy A. K., Mac Low M. M., Walter F., Kennicutt R. C., Brinks E., de Blok W. J. G., 2009, AJ, 137, 4424
Tasker E. J., Tan J. C., 2009, ApJ, 700, 358
Teyssier R., 2002, A&A, 385, 337
Thornton K., Gaudlitz M., Janka H. T., Steinmetz M., 1998, ApJ, 500, 95
Toomre A., 1964, ApJ, 139, 1217
Vandervoort P. O., 1970, ApJ, 161, 87
Walter F., Brinks E., de Blok W. J. G., Bigiel F., Kennicutt R. C., Jr, Thornley M. D., Leroy A., 2008, AJ, 136, 2563
Zhang H. X., Hunter D. A., Elmegreen B. G., 2012, ApJ, 754, 29

This paper has been typeset from a \TeX/L\AA\TeX file prepared by the author.